Journal of Neuroscience Research 84:1778–1788 (2006)

Contribution of Valine 7′ of TMD2 to Gating of Neuronal α3 Receptor Subtypes

Madeline Nieves-Cintrón,[1] Daniel Caballero-Rivera,[2] Manuel F. Navedo,[1] and José A. Lasalde-Dominicci[1]★

[1]Department of Biology, University of Puerto Rico, Rio Piedras Campus, San Juan, Puerto Rico
[2]Department of Chemistry, University of Puerto Rico, Rio Piedras Campus, San Juan, Puerto Rico

The second transmembrane domain (TMD2) of the Cys-loop family of ligand-gated ion channels forms the channel pore. The functional role of the amino acid residues contributing to the channel pore in neuronal nicotinic α3 receptors is not well understood. We characterized the contribution of TMD2 position V7′ to channel gating in neuronal nicotinic α3 receptors. Site-directed mutagenesis was used to substitute position α3 (V7′) with four different amino acids (A, F, S, or Y) and coexpressed each mutant subunit with wild-type (WT) β2 or β4 subunits in *Xenopus* oocytes. Whole-cell voltage clamp experiments show that substitution for an alanine, serine, or phenylalanine decreased by 2.3–6.2-fold the ACh-EC_{50} for α3β2 and α3β4 receptor subtypes. Interestingly, mutation V7′Y did not produce a significant change in ACh-EC_{50} when coexpressed with the β2 subunit but showed a significant approximately two-fold increase with β4. Similar responses were obtained with nicotine as the agonist. The antagonist sensitivity of the mutant channels was assessed by using dihydro-β-erythroidine (DHβE) and methyllycaconitine (MLA). The apparent potency of DHβE as an antagonist increased by ~3.7- and 11-fold for the α3β2 V7′S and V7′F mutants, respectively, whereas no evident changes in antagonist potency were observed for the V7′A and V7′Y mutants. The V7′S and V7′F mutations increase MLA antagonist potency for the α3β4 receptor by ~6.2- and ~9.3-fold, respectively. The V7′A mutation selectively increases the MLA antagonist potency for the α3β4 receptor by ~18.7-fold. These results indicate that position V7′ contributes to channel gating kinetics and pharmacology of the neuronal nicotinic α3 receptors.

Key words: AChR; nicotine; acetylcholine

Neurotransmitter gated channels are key components of the communication process between neurons, i.e., synaptic transmission. Upon agonist binding, the receptor undergoes a series of conformational changes leading to opening of the ion channel pore, flux of specific ions into the cell, and inactivation (desensitization) of the channel after prolonged exposure to the agonist. Nicotinic acetylcholine receptors (nAChRs) are members of a superfamily of neurotransmitter-gated ion channels, which includes γ-aminobutyric acid type A ($GABA_A$), glycine, and 5-hydroxitryptamine-3 ($5\text{-}HT_3$) receptors. These receptors share a pentameric structure, with each subunit in the pentamer contributing to the formation of an ion pore. The subunits making up the pentamer have a common topology; each subunit has a large extracellular N-terminal domain, four transmembrane domains (TMD1–TMD4), and a C-terminal domain. The binding site for the neurotransmitter is located at the subunit interfaces in the extracellular N-terminal domain.

Much effort has been expended in the identification of key amino acid residues that modulate nAChR function. Structure and function studies, carried out at the amino acid level, have shown that alterations of the primary structure of the nAChR lead to disruption (either gain or loss) of receptor function (Karlin, 2002). For example, site-directed mutagenesis of amino acid residues at transmembrane domain 2 (TMD2) can change the selectivity of the ion channel from a cationic to an anionic one (Corringer et al., 1999). In the neuronal nAChR subunits α3, α4, β2, and β4, the first and second transmembrane domains have been shown to influence agonist binding and efficacy (Rush et al., 2002). Also, mutations at TMD2 of α4 and β2 neuronal subunits have been reported to alter conductance, permeability, and gating and to cause nocturnal frontal lobe epilepsy (ADNFLE; Kuryatov et al., 1997). Furthermore, single-amino-acid changes at TMD2 of muscle-type nAChRs cause inappropriate function of the receptor (e.g., altered desensitization, potency, conductance, and

Madeline Nieves-Cintrón's and Manuel F. Navedo's current address is Department of Physiology and Biophysics, University of Washington School of Medicine, Seattle, WA 98195.

Contract grant sponsor: NIH; Contract grant number: RO1GM56371-5; Contract grant number: GM08102-27.

★Correspondence to: José A. Lasalde-Dominicci, Department of Biology, University of Puerto Rico, P.O. Box 23360, San Juan, PR 00931-3360. E-mail: joseal@coqui.net

Received 28 March 2006; Revised 17 July 2006; Accepted 9 August 2006

Published online 16 October 2006 in Wiley InterScience (www.interscience.wiley.com). DOI: 10.1002/jnr.21085

gating) that produces slow channel congenital myasthenic syndrome (SCCMS; Ohno and Engel, 2002).

In this work, we examined the contribution of position V7′ in TMD2 of the neuronal nAChR α3 subunit to the function of the channel. Position V7′ was of particular interest because of its high degree of conservation among different neuronal α subunits. Previously, a mutation of the homologous position in TMD2 of the muscle α subunit (V249F) has been shown to produce an SCCMS (Milone et al., 1997). To characterize the structural and functional elements of position V7′ in TMD2 of the neuronal α3 subunit, different amino acid residues (A, F, S, and Y) were substituted at this position. We used electrophysiology measurements to determine the effect of these mutations on ion channel function. Our results support a contribution of position V7′ to ion channel gating and pharmacology of the α3 neuronal nAChR subtype.

MATERIALS AND METHODS

Generation of α3 Subunit Mutations

Only neuronal α and β subunits from *Rattus norvegicus* were used in this study. α3, β2, and β4 clones (GeneBank Nos. L31621, L31622, and U42976, respectively) were kindly provided by Dr. Jim Patrick (Baylor College of Medicine). The coding region of the α3 of the rat neuronal AChR was subcloned into the EcoRI/Hind III site of the pcDNA3 vector under the T7 promoter (Promega, Madison, WI). Amino acid side chain substitutions at position V7′ (α3: V7′A, V7′S, V7′F, and V7′Y) were prepared by using the Quik-Change Site Directed Mutagenesis Kit (Stratagene, La Jolla, CA). Oligonucleotide primers containing the desired mutation were generated (Invitrogene). Sample reactions were prepared as instructed by the manufacturer. The mutant DNA was then transformed into Epicurian Coli XL1-Blue supercompetent cells. The successful inclusion of mutations was confirmed by DNA sequence analysis performed at the DNA Sequencing Facility in the Section of Evolution and Ecology, University of California, Davis. All pcDNA3 plasmids containing the coding region of the desired neuronal subunit were linearized with the EcoRI site, and cRNA was produced by using the T7 mMessage mMachine Kit (Ambion, Austin, TX). The integrity and quantity of each cRNA were verified by gel electrophoresis, weight markers, and by spectrophotometry.

nAChR Expression in *Xenopus* Oocytes

Stage V–VI oocytes were extracted from *Xenopus laevis* in accordance with the guidelines of the University of Puerto Rico Institutional Animal Care and Use Committee. The oocytes were incubated in collagenase type IA (Sigma-Aldrich, St. Louis, MO) to remove the follicles. The enzymatic treatment was followed by manual defolliculation to remove any remaining follicles. Single oocytes were injected within 1 hr with 40 nl of cRNA at a ratio of 2α:3β. The cRNA mixtures were pressure injected with a positive displacement injector (Drummond Instruments, Broomhall, PA), and the injected oocytes were incubated at 19°C in 0.5× Leibovitz's L-15 medium (Invitrogene) supplemented with 400 μg/ml bovine serum albumin and 10 mg/liter antibiotic/antimycotic (Invitrogene). The incubation medium was changed daily. Electrophysiology experiments were carried out 3 days after cRNA injection.

Electrophysiological Recordings

The Gene Clamp 500 amplifier (Axon Instruments, Foster City, CA) in its two-electrode voltage-clamp configuration was used to record agonist-induced currents. The electrodes were pulled with a vertical pipette puller (model PP-830; Narishige). Electrodes with resistance <10 MΩ were used to record voltage. Current electrodes had a resistance of <2 MΩ. Electrodes were filled with 3 M KCl. Impaled oocytes in the recording chamber were perfused at a rate of 10.0 ml/min with MOR-2 buffer [115 mM NaCl, 2.5 mM KCl, 5 mM $MgCl_2$, 1 mM Na_2HPO_4, 5 mM *N*-(2-hydroxyethyl)piperazine-*N*′-2-ethanesulfonic acid (HEPES), and 0.2 mM $CaCl_2$ (pH 7.4)]. Membrane potential was held at −70 mV, unless otherwise indicated. Membrane currents were digitalized at 2 kHz with an Axon Digidata 1200 interface (Axon Instruments) and recorded with the Whole Cell Program 2.3 (kindly provided by Dr. J. Dempster) running on a Pentium III-based computer.

Concentration-response data were collected from peak currents at seven agonist concentrations (in μM 0.1, 1, 3, 10, 30, 100, and 300). We employed two different agonists, ACh and nicotine. GraphPad Prism software (GraphPad Software, San Diego, CA) was used to perform a nonlinear regression fit with a sigmoidal concentration-response variable slope equation (Ortiz-Acevedo et al., 2004):

$$I = I_{\min} + \frac{I_{\max} - I_{\min}}{1 + 10^{((\log EC_{50} - \log[agonist]) \cdot nH_{app})}}, \qquad (1)$$

where I is the macroscopic current at a given agonist concentration; I_{max} and I_{min} are the maximum and minimum responses recorded, respectively; EC_{50} is the agonist concentration required to achieve half-maximal response, and [agonist] is the concentration of agonist. The apparent Hill coefficient (nH_{app}) was determined from the Hill plot by a linear regression of $\log[I_{peak}/(I_{max} - I_{peak})]$ against the log[agonist] (Cohen et al., 1995). In this Hill plot, I_{peak} is the ACh-induced current recorded at each agonist concentration, and I_{max} is the maximal response observed in each experiment. The average slope value (nH) of the Hill plot calculated as described above for each wild-type (WT) and mutant receptor subtype was used to fix the nH_{app}, whereas I_{max} and EC_{50} values were allowed to vary when fitting to the Hill equation. The EC_{50} values for individual oocytes were averaged to generate final estimates. EC_{50} estimated errors are provided as 95% confidence intervals (95% CI). To determine the possible effect of agonist-induced desensitization and/or channel block on the EC_{50} and Hill estimates obtained from full concentration-response curves, we plot the log of peak currents elicited by low [agonist] (0.1, 1, 3, 10 μM) against the log [agonist]. The slope of the log-log plot approximates the Hill coefficient (Connolly et al., 1992; Cohen et al., 1995).

Because some mutant receptors showed a decline in peak current at high nicotine concentrations, we used the following model based on a Gaussian curve shape to fit nicotine data and to represent better the decline in peak current amplitude (Christopoulos et al., 2001):

$$E = basal + range \times e - \left[\frac{10^{\log[A]} - midA}{slope}\right]^2, \quad (2)$$

where

$$midA = \log EC_{50} + slope\sqrt{-\ln(0.5)}. \quad (3)$$

Basal is the minimal response; midA represents the logarithm of agonist concentration causing the response halfway between basal and the top of the dip in the curve (i.e., the log EC_{50}), and range denotes the maximal response from basal to the top of the dip in the curve. It is important to note that the slope parameter in the preceding equations is not the same as the Hill slope (nH) found in sigmoidal C/R curves. The slope parameter in the Gaussian is a constant that allows the fitting of the curves. Even though the described Gaussian distribution is not a mechanistic model, it provides an empirical way to fit our data and to obtain parameters that can be compared between receptor subtypes and agonists. This kind of analysis has been previously used to fit C/R data (Christopoulos et al., 2001).

Inhibition curves were generated by coapplication of 10 μM ACh and increasing concentrations (in μM 0.001, 0.01, 0.1, 1, 3, 10, 30, and 300) of the proper antagonist. Inhibition curves were fitted with the equation:

$$I = \frac{I_{\max}}{\left[1 + \left(\frac{IC_{50}}{[antagonist]}\right)\right]}, \quad (4)$$

where I is the current at a given antagonist concentration, I_{max} is the current in the absence of antagonist, IC_{50} is the concentration of antagonist needed to cause 50% inhibition of the agonist response, and [antagonist] is the concentration of antagonist. The values from inhibition curves were obtained in a way similar to that used for agonist experiments. A system-independent estimate of the apparent antagonist potency (apparent K_B) was performed from an estimate of the IC_{50} corrected for the level of agonism (10 μM ACh) by using a modified Cheng-Prusoff equation (Leff and Dougall, 1993):

$$K_B = \frac{IC_{50}}{\left[\left(2 + \left(\frac{[agonist]}{EC_{50}}\right)^{nH_{app}}\right)^{\frac{1}{nH_{app}}} - 1\right]}, \quad (5)$$

where K_B is the apparent antagonist potency, IC_{50} is the concentration of antagonist needed to cause 50% inhibition of the agonist response, EC_{50} is the agonist concentration required to achieve half-maximal response, [agonist] is the concentration of agonist, and nH_{app} is the apparent Hill slope.

Muscle Subunits

α1	MILSLS V LLSLTVFLLVIV
β1	MGLSIF A LLTLTVFLLLLA
δ	TSVALS V LLAQSVFLLLIS
ε	CTVSIN V LIAQTVFLFLIA

Rat Neuronal Subunit

α2	ITLCIS V LLSLTVFLLLIT
α3	VTLCIS V LLSLTVFLLVIT
α4	ITLCIS V LLSLTVFLLLIT
β2	MTLCIS V LLALTVFLLLIS
β4	MTLCIS V LLALTFFLLLIS

Fig. 1. Primary structure of the nicotinic acetylcholine receptor TMD2. Amino acid sequence alignment of the TMD2 of different neuronal α and β subunits and muscle α, β, γ, and ε subunits. Note the high degree of conservation of position V7′ among the different subunits.

To determine the effect of the mutations on the cumulative desensitization, successive applications of a 300 μM ACh solution were applied for 6 sec, every 5 min, for a period of 20 min. Peak currents from successive applications of a 300 μM ACh solution were normalized to maximal current obtained during the first ACh application. The membrane potential was held at −70 mV for these experiments.

Chemicals

All chemicals, including agonists and antagonists, were purchased from Sigma-Aldrich (St. Louis, MO).

Statistical Analysis

Data are presented as mean ± SEM. EC_{50} and IC_{50} estimated errors are provided as 95% confidence intervals. Two-sample comparisons were made by using a Student's *t*-test or a Wilcoxon signed-rank test. For more than two groups, an ANOVA with a Dunnett's post-test analysis was used. $P < 0.05$ was considered significant.

RESULTS

Amino Acid Substitution at TMD2

Figure 1 compares the amino acid sequence for several M2 domains in the α3 subunit TMD2. Position V7′ is an amino acid residue that is highly conserved among different neuronal α and β subunits and in the muscle α, δ, and ε subunits (Fig. 1). This observation indicates that this position may be important for proper channel function. Indeed, a spontaneous mutation at the homologous position in the muscle α-TMD2 was reported to produce a form of congenital myasthenic syndrome (Milone et al., 1997), strengthening the hypothesis that this position is important for proper channel function. To characterize the structural and functional contributions of position α3V7′, four amino acid replacements were made. We chose amino acid residues

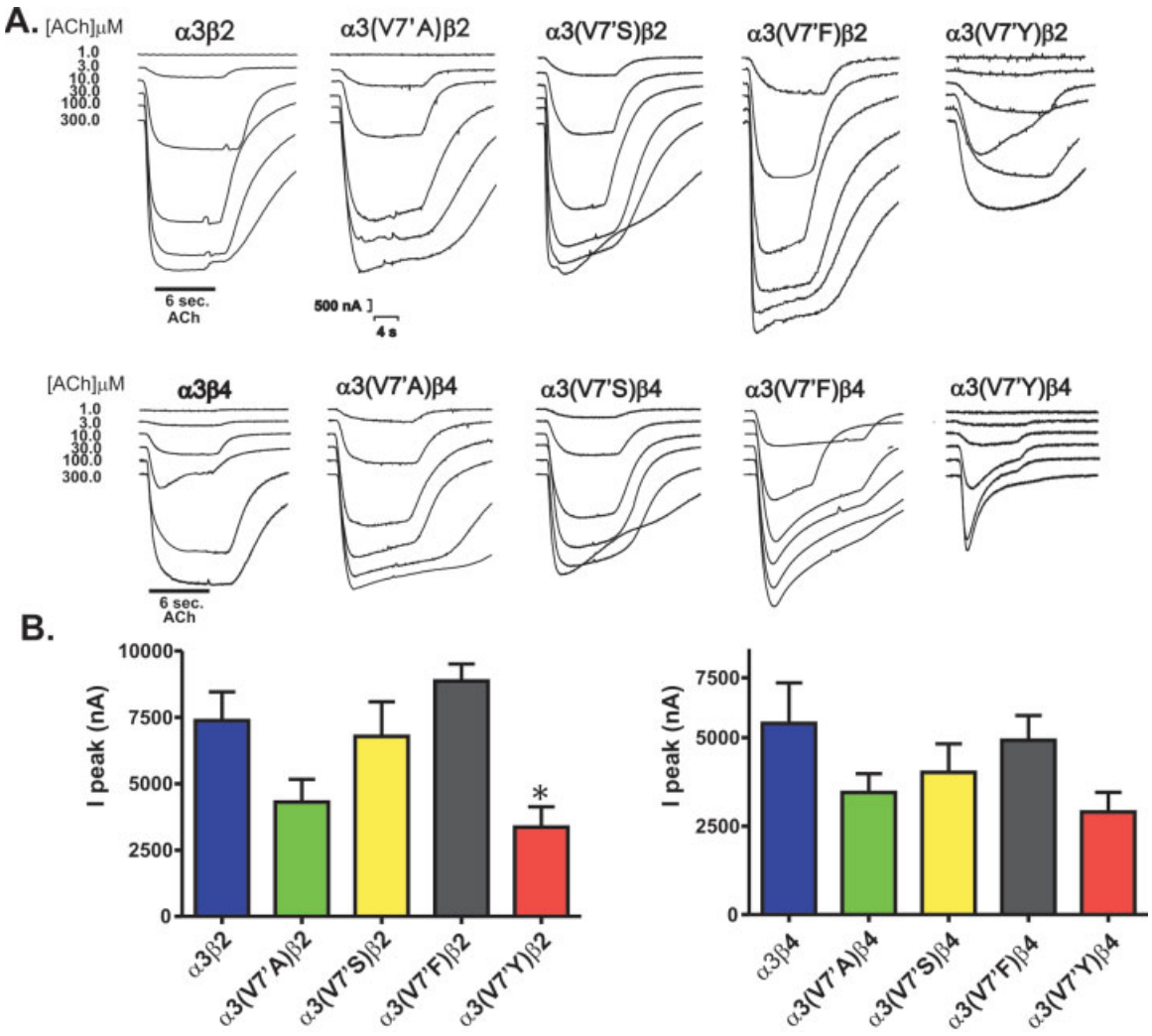

Fig. 2. Functional consequences of amino acid substitution at position α3V7′. **A:** Representative ACh-induced currents recorded from wild-type and mutant α3 nAChR subtypes. **B:** Bar plot of peak current response obtained after stimulation of each WT and mutant receptor subtype with 300 μM ACh. $^{\star}P < 0.05$ compared with response in WT. Results are summarized in Table I.

that would alter the amino acid volume but conserve polarity (V7′A and V7′F) and would change amino acid volume and polarity (V7′S) and a residue that, as with phenylalanine, would increase the volume but render the position less hydrophobic than phenylalanine (V7′Y). All mutations were coexpressed with β2 or β4 WT subunits in *Xenopus laevis* oocytes, and the receptor's functional properties were evaluated with the two-electrode voltage-clamp technique.

First, we examined the whole-cell maximal response of *Xenopus* oocytes expressing WT or mutant neuronal AChRs with a maximal efficacious concentration of ACh (300 μM) at −70 mV. All the mutations examined produced functional channels (Fig. 2). The maximal responses to ACh were similar in WT and α3(V7′F) receptor subtypes (Fig. 2A,B). ACh-induced responses were normalized to the maximal response, and the results were used to generate the concentration-response curves. We fitted ACh concentration-response data to the Hill equation (Eq. 1) with the nH_{app} for each WT and mutant receptor subtype as determined from the Hill plot of ACh responses (see Materials and Methods). The V7′F mutation produced a decrease in EC_{50} of about 6.2-fold when coexpressed with β2 and a 3.7-fold decrease when coexpressed with β4 WT subunits (Fig. 3A,B, Table I).

The V7′A and V7′S mutant receptors showed a decrease in EC_{50} of about 2.6- and 2.3-fold, respectively, when expressed with β2, whereas α3(V7′Y)β2 did not significantly affect ACh EC_{50} (Fig. 3B, Table I). The coexpression of the V7′A and V7′S mutants with β4 produced a significant decrease of 4.6- and 5.3-fold

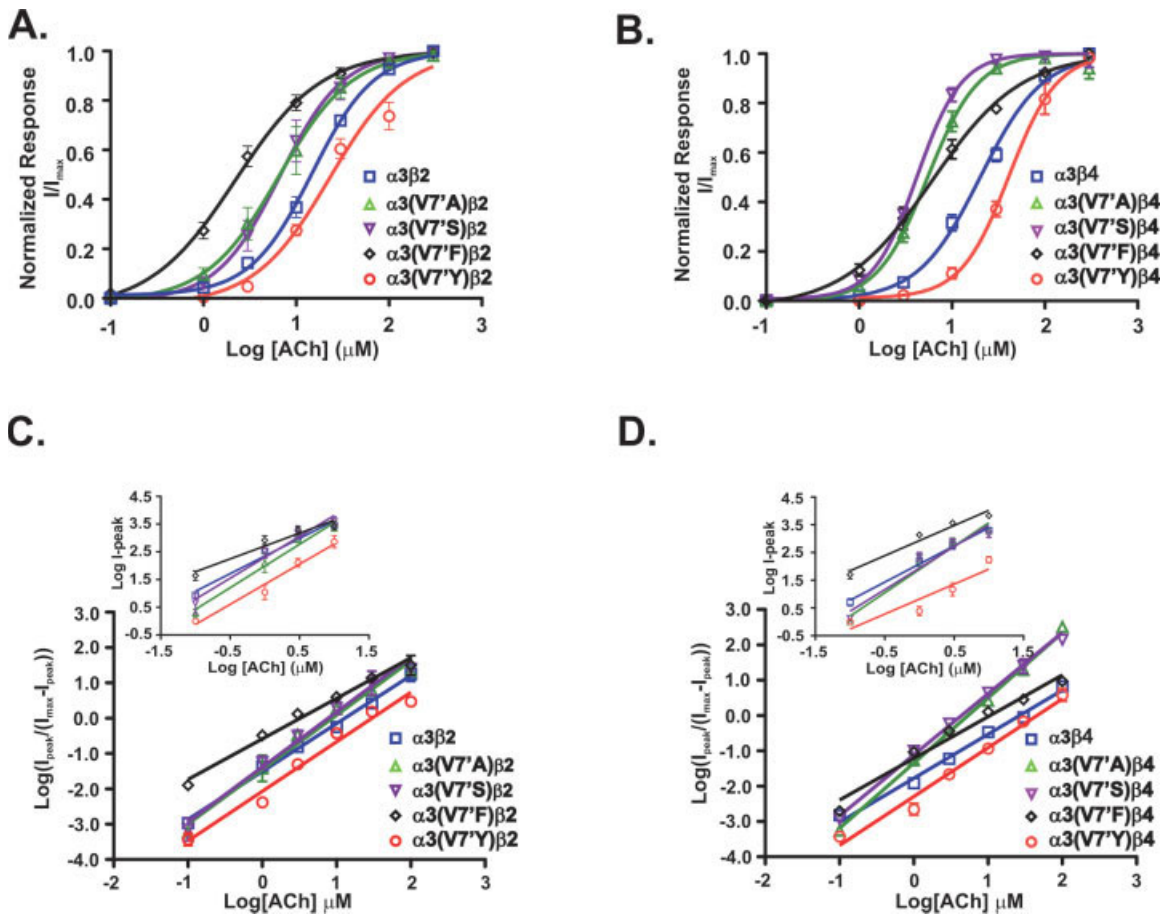

Fig. 3. Effect of amino acid substitution at position 7′ in the concentration-response relationship for ACh. Concentration-response data for α3β2 (**A**) and α3β4 (**B**) and mutant α3 receptor subtypes were collected from peak currents at seven ACh concentrations (0.1, 1, 3, 10, 30, 100, and 300 μM). Each concentration-response curve was normalized to maximal current for each oocyte tested. Error estimation for EC_{50} values is presented as 95% CI. Hill plots for α3β2 (**C**) and α3β4 (**D**) WT and mutant receptors subtypes determined from the linear regression of $\log[(I_{peak}/(I_{max} - I_{peak})]$ vs. log[agonist]. The **insets** show log-log plots of peak currents elicited by low agonist concentrations.

in ACh EC_{50}, respectively, whereas the V7′Y mutant caused a significant 2.2-fold increase in ACh EC_{50} ($P = 0.01$ compared with WT; Fig. 3B, Table I).

We determined apparent Hill coefficients (nH_{app}) from log-log plots at low ACh concentrations (Connolly et al., 1992; Cohen et al. 1995) to analyze the possible effects of desensitization and channel block on full concentration-response curves (Fig. 3C,D). The nH_{app} obtained form log-log plots were similar to the values obtained from full curves (α3β2, 1.2 ± 0.05; V7′A, 1.6 ± 0.14; V7′S, 1.5 ± 0.18; V7′F, 0.92 ± 0.1; and V7′Y, 1.4 ± 013). The same is true for α3β4 receptors subtypes (α3β4, 1.3 ± 0.01; V7′A, 1.6 ± 0.2; V7′S, 1.4 ± 0.18; V7′F, 1.2 ± 0.2; and V7′Y, 1.3 ± 0.13), although, upon consecutive stimulation with 300 μM ACh, some mutants showed increased desensitization compared with WT (see below). The similarity of the nH from log-log plots at low agonist concentrations and that from full Hill plots (Table I) shows that desensitization did not affect the nH_{app} or the EC_{50} obtained from peak currents elicited by the systematic application of a full range of agonist concentrations to single cells. Thus, the observed decrease in EC_{50} responds to a functional effect of the mutations on the receptors.

We found that V7′A and V7′S, as well as the V7′F mutation, did not produce a significant change in the magnitude of the macroscopic response whether coexpressed with β2 or β4 WT subunits (Fig. 2B, Table I). Conversely, the α3(V7′Y)β2 and α3(V7′Y)β4 mutant receptors showed a significant decrease in the macroscopic response. We decided to evaluate the effect of these mutations on the time course of receptor cumulative desensitization by using successive stimulations with 300 μM ACh (see Materials and Methods). Even though the traces in Figure 2A did not show very pronounced desensitization, the WT α3β2 receptor displayed a faster current decay than α3β4 WT receptors when successively challenged with 300 μM ACh, which is consistent with previous results from Nelson and Lindstrom (1999; Fig. 4A,B). When coexpressed with β2, only V7′S pro-

TABLE I. Functional Characterization of Mutant α3 Receptor Subtypes[†]

	ACh response				Nicotine response			
nAChR	n	EC_{50} (μM)[a]	nH_{app}	I peak (nA)[b]	n	EC_{50} (μM)[c]	nH_{app}	I peak (nA)[d]
α3β2	7	15.6 (13.5–17.0)	1.4 ± 0.05	7,370 ± 1,086	7	16.5 (13.5–19.7)	1.3 ± 0.10	4,008 ± 692
α3(V7′A)β2	7	5.9★ (4.0–8.0)	1.5 ± 0.1	4,304 ± 869	5	5.7★ (5.6–7.8)	2.0 ± 0.20	2,936 ± 530
α3(V7′S)β2	5	6.8★ (5.1–8.0)	1.5 ± 0.1	6,780 ± 1,299	5	2.9★ (2.3–3.6))	2.3 ± 0.20	3,555 ± 612
α3(V7′F)β2	13	2.5★ (1.7–2.7)	1.1 ± 0.1	8,862 ± 648	7	3.2★ (2.6–3.9)	1.6 ± 0.08	5,765 ± 806
α3(V7′Y)β2	5	20.1 (15.5–21.4)	1.4 ± 0.06	3,369 ± 765★	6	23.3 (22.0–25.3)	1.3 ± 0.07	596 ± 105★
α3β4	7	22.1 (19.1–25.0)	1.2 ± 0.04	5,349 ± 1,788	7	28.3 (19.3–33.5)	1.2 ± 0.04	3,008 ± 993
α3(V7′A)β4	5	5.2★ (4.0–6.1)	1.8 ± 0.06	3,210 ± 422	5	4.3★ (3.0–6.3)	2.3 ± 0.20	3,964 ± 1,113
α3(V7′S)β4	5	4.2★ (3.5–4.6)	1.7 ± 0.05	4,016 ± 802	9	4.7★ (3.9–5.4)	2.4 ± 0.10	5,301 ± 284
α3(V7′F)β4	11	6.0★ (5.0–7.0)	1.2 ± 0.05	4,925 ± 699	7	4.0★ (3.6–4.0)	1.5 ± 0.12	2,762 ± 863
α3(V7′Y)β4	5	48.4★★ (36.1–58.0)	1.4 ± 0.06	2,898 ± 554	5	49.7★ (40.7–58.7)	1.1 ± 0.08	563 ± 268★

[†]Errors for EC_{50} values are given as 95% confidence intervals; nH_{app} values are given as the mean ± SEM. The n for each experiment is indicated in the table.
[a]ACh EC_{50} was determined by using Eq. 1.
[b]Peak currents for ACh were obtained by averaging the macroscopic responses of individual oocytes at 300 μM ACh.
[c]Nicotine EC_{50} was determined from Eq. 2.
[d]Peak responses for nicotine were obtained by averaging the macroscopic response of individual oocytes elicited by 30 μM nicotine.
★$P < 0.05$ vs. response in WT receptor.
★★$P < 0.01$ vs. response in WT receptor.

duced a significant rundown in peak current ($P < 0.05$ compared with WT), and no statistically significant difference was observed for α3(V7′A)β2, α3(V7′F)β2, or α3(V7′Y)β2 mutant receptors. The α3V7′A, α3V7′S, α3V7′Y, and α3V7′F mutant subunits expressed with the β4 WT subunit showed a significant increase in current decay time in comparison with the WT α3β4 receptor subtype ($P < 0.001$; Fig. 4B). Although the macroscopic response of α3(V7′Y)β4 was smaller and decayed faster than that of the WT α3β4 receptor (Fig. 2A), the cumulative desensitization was less than that of the other mutations (Fig. 4B).

Position 7′ at TMD2 Contributes to α3 Receptor Subtype Pharmacology

We characterized the effect of the amino acid substitutions on the pharmacology of nicotine. Figure 5 shows representative current traces elicited by the application of a range of nicotine concentrations (Fig. 5A).

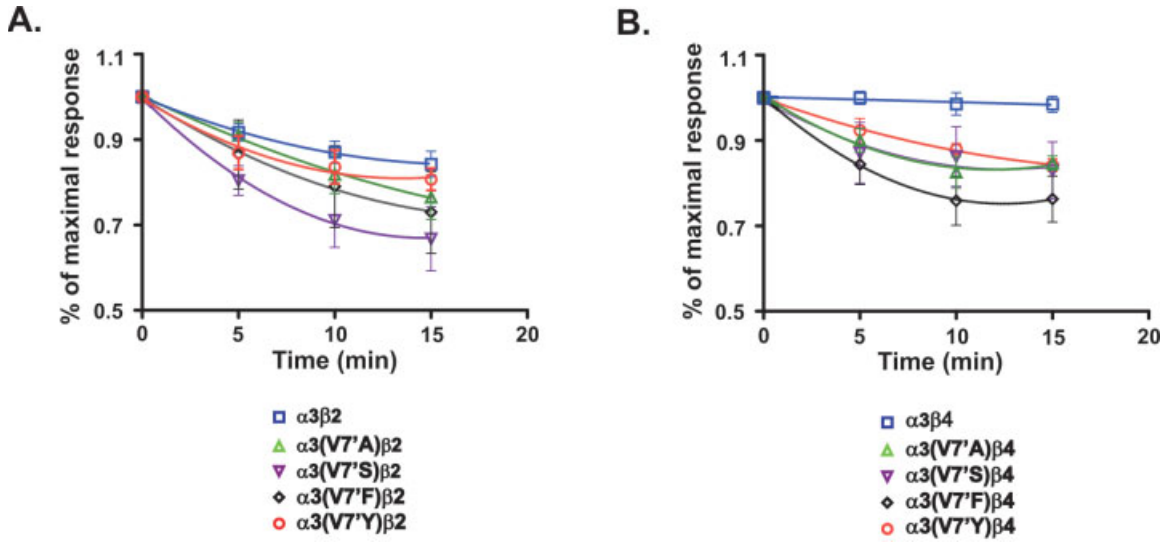

Fig. 4. Effects of amino acid substitution at position V7′ on α3 receptor subtypes desensitization. Time course of peak current rundown of α3β2 (**A**) and α3β4 (**B**) WT and mutant receptors, after successive stimulation with 300 μM ACh. Peak current rundown curves were normalized to maximal current obtained during the first ACh application. Data are expressed as mean ± SEM of six to 12 individually tested oocytes. $P < 0.001$ for mutant receptors coexpressed with the β4 WT subunit when compared with response in WT. $P < 0.05$ for α3(V7′S)β2 when compared with response in WT.

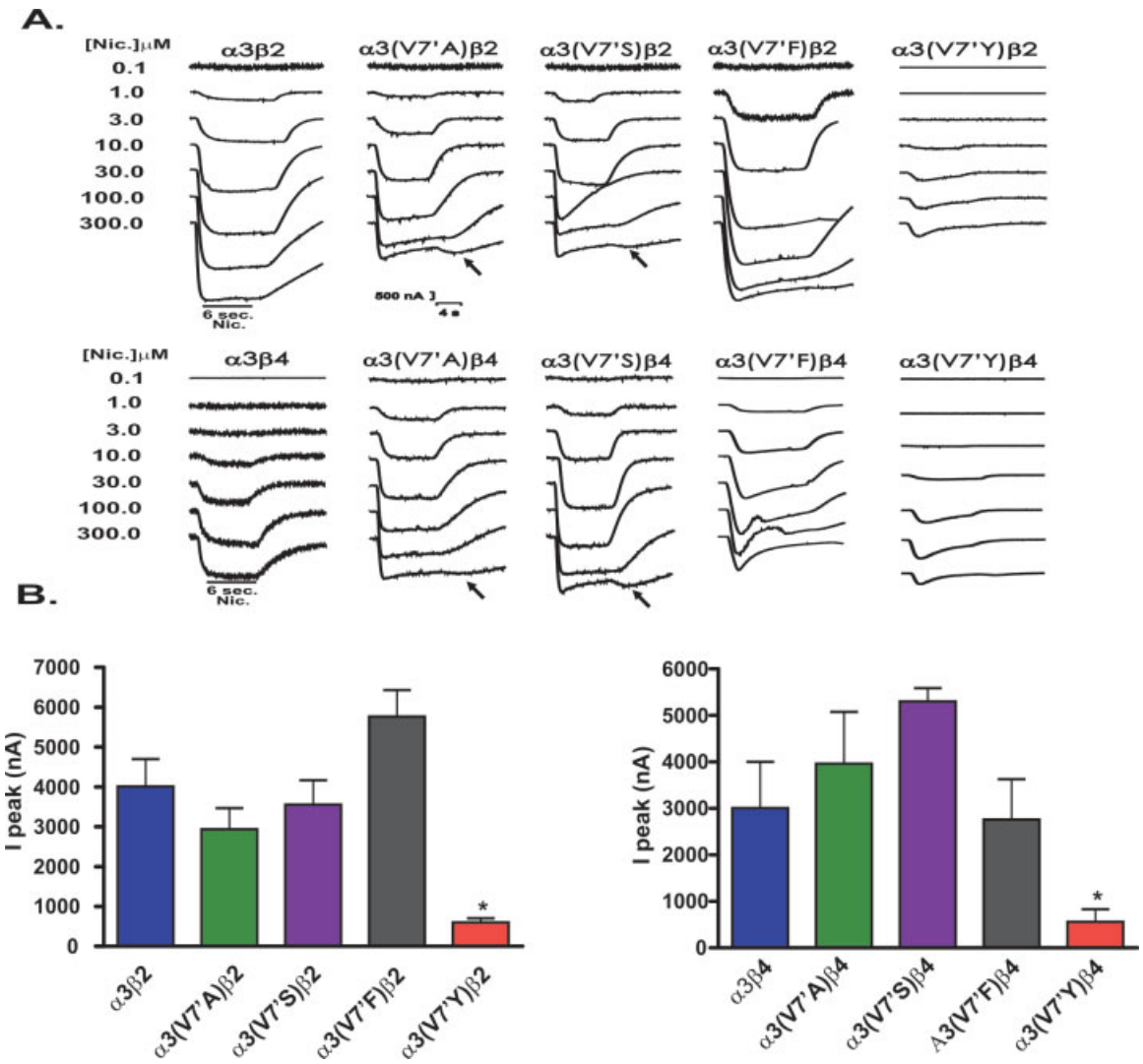

Fig. 5. Functional consequences of amino acid substitution at position α3V7′ on the pharmacology of nicotine. **A:** Representative nicotine-induced family of currents recorded from WT and mutant α3 nAChR subtypes. **B:** Bar plot of peak current response obtained after stimulation of each WT and mutant receptor subtype with 30 μM nicotine. ⋆$P < 0.05$ compared with response in WT. Results are summarized in Table I.

All the mutations showed response to nicotine, and peak currents were observed at 30 μM nicotine (Fig. 5B). However, we observed that the maximal response for some of the constructs (V7′A, V7′S and V7′F) was always produced at lower nicotine concentrations, whereas, at high nicotine concentrations (100–300 μM), the macroscopic response was decreased (Fig. 5A, Table I). Also, we observed rebound currents upon wash out of high concentrations of nicotine (300 μM) in several traces (see arrows in Fig. 5A). This phenomenon suggests that agonist blocking is occurring, which might explain the reduction in macroscopic response observed upon application of high nicotine concentrations.

Figure 6A,B shows concentration-response curves for nicotine. We did not fit nicotine and ACh data with the same equation because of the described declines in peak current amplitude at higher nicotine concentrations. Rather, we fitted nicotine data to an empirical model (Eq. 2, 3) that allowed us to determine the nicotine EC_{50} (Table I).

Nicotine-elicited peak currents were used to generate concentration-response curves. We observed that the α3(V7′A)β2, α3(V7′S)β2, and α3(V7′F)β2 mutant receptors shifted the C/R curves to the left, decreasing nicotine EC_{50} by 2.9-, 5.7-, and 5.2-fold, respectively. Also, these mutant receptors showed a clear bell-shaped profile, reflecting the observed decline in peak current amplitudes at high nicotine concentrations (100–300 μM; Fig. 6A, Table I). In contrast, nicotine EC_{50} was not significantly different for the α3(V7′Y)β2 receptor

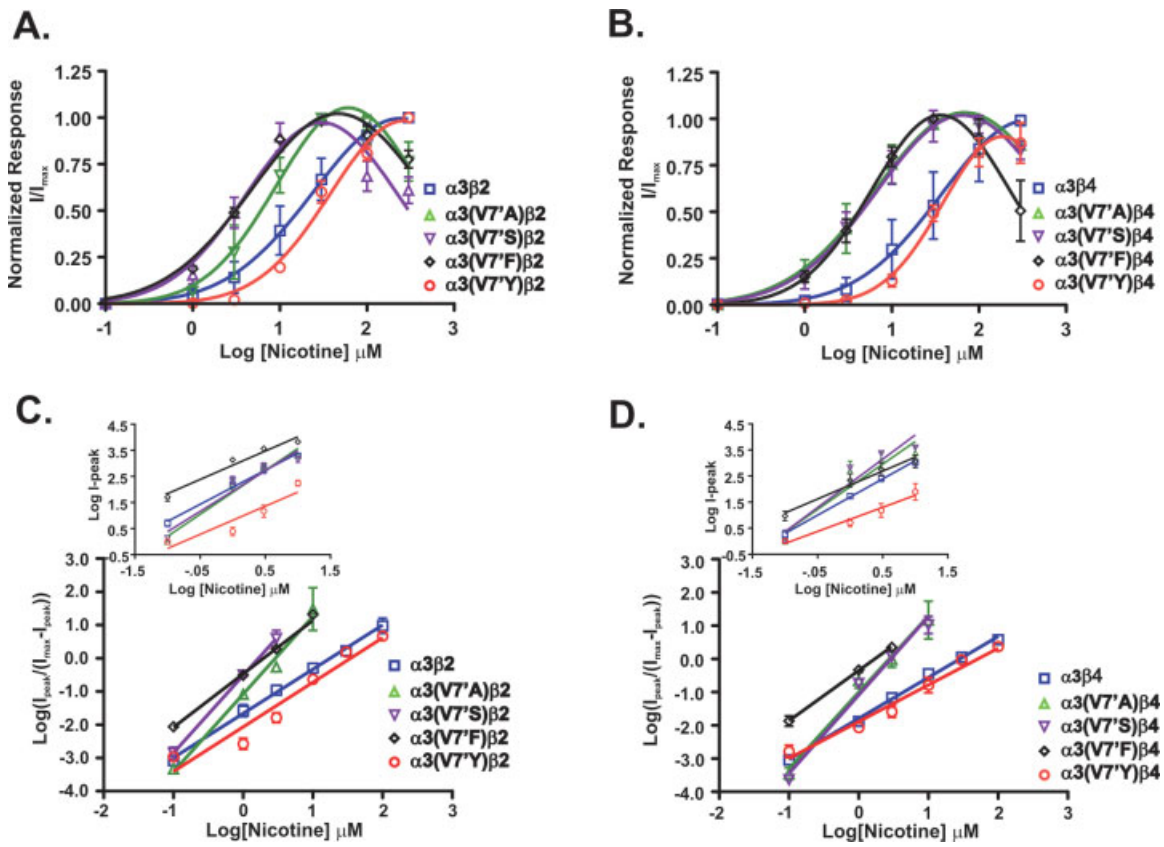

Fig. 6. Effects of amino acid substitution at position 7′ on nicotine-induced activation of neuronal α3β2 and α3β4 receptors. Concentration-response curves for the WT and mutant α3β2 (**A**) and WT and mutant α3β4 (**B**) receptors. Seven different concentrations of nicotine were used to generate the curves (0.1, 1, 3, 10, 30, 100, and 300 μM). Data points were fitted using Eq. 3 and 4. Error estimates for EC_{50} values are given as 95% CI. Results are summarized in Table I. Hill plots for α3β2 (**C**) and α3β4 (**D**) WT and mutant receptors subtypes determined from the linear regression of log $[I_{peak}/(I_{max} - I_{peak})]$ vs. log [agonist]. The **insets** show log-log plots of peak currents elicited by low agonist concentrations.

(Fig. 6A, Table I). Coexpression of α3(V7′A) and α3(V7′S) with the β4 WT subunit caused a 6.6- and 6.0-fold reduction in the EC_{50} for nicotine, respectively, whereas the α3 (V7′F) construct produced a 7.1-fold decrease in nicotine EC_{50} (Fig. 6B, Table I). Mutation V7′Y, however, produced a 1.8-fold increase in the EC_{50} for nicotine, when coexpressed with β4 WT subunit, that was consider to be significant ($P < 0.05$; Fig. 6B, Table I). A decline in peak current amplitudes at high nicotine concentrations is also obvious in the curves of these receptor subtypes (Fig. 6B).

Because some mutations showed an apparent channel block, we explored whether channel block or desensitization was having an effect on the results obtained from our full C/R curves. The same approach used for ACh data was employed. Briefly, we determined the nH from the slope of log-log plots at low nicotine concentrations (0.1, 1, 3, and 10; Fig. 6C,D, Table I). The estimated nH obtained did not differ from the values from the full Hill plot (α3β2, 1.3 ± 0.08; V7′A, 1.7 ± 0.24; V7′S, 1.6 ± 0.30; V7′F, 1.1 ± 0.2; and V7′Y, 1.1 ± 0.3). For α3β4 receptor subtypes, the estimated nH were (α3β4, 1.4 ± 0.04; V7′A, 1.7 ± 0.4; V7′S, 1.9 ± 0.4; V7′F, 1.1 ± 0.1; and V7′Y, 0.9 ± 0.10). The similarity between the nH from Hill plot curves and log-log plots at low agonist concentrations suggests not that desensitization and channel block are responsible for the differences in EC_{50} observed between the WT and the mutant receptors but that they are due to functional effects of the mutation on the receptor.

Influence of V7′ on Competitive Antagonist Sensitivity

To test whether the mutations at position V7′ affect the sensitivity of the channel to competitive antagonist inhibition, we generated inhibition curves of ACh-elicited currents in the presence of a competitive antagonist. For α3β2 and α3β4 WT and mutant receptors, a fixed concentration of ACh (10 μM) was coapplied with increasing concentrations of the competitive antagonists dihydro-β-erythroidine (DHβE) and methyllycaconitine (MLA), respectively. The apparent potency of the DHβE antagonist increased by ∼3.7- and 11-fold for

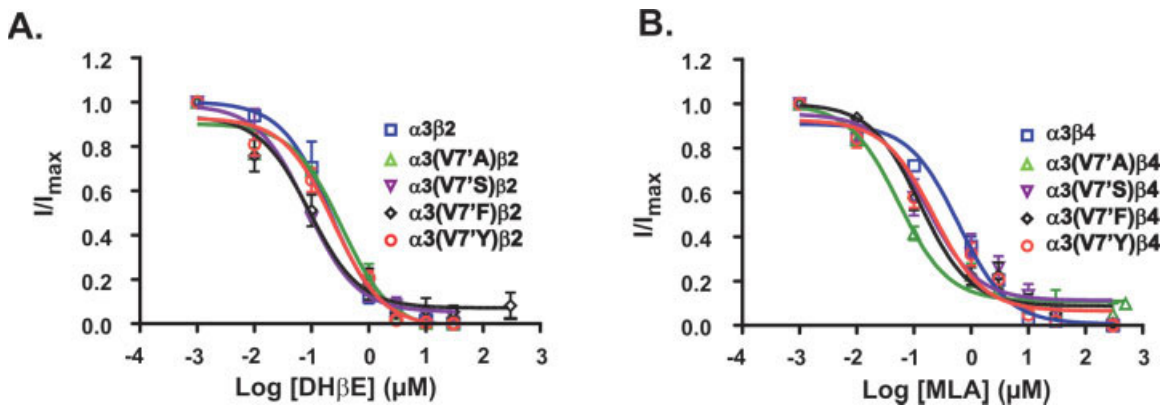

Fig. 7. Effect of α3V7′ mutations on the competitive antagonist sensitivity of α3β2 and α3β4 receptor subtypes. Two-electrode voltage clamp was used to measure the responses of the WT and mutant receptors to ACh in the presence of a competitive antagonist. **A:** Response of oocytes expressing WT α3β2 or the α3(V7′X)β2 series of mutant receptors to coapplication of increasing concentrations of DHβE and a fixed concentration of ACh (10 μM). **B:** Response of oocytes expressing WT α3β4 or the α3(V7′X)β4 series of mutant receptors to coapplication of increasing concentrations of MLA and a fixed concentration of ACh (10 μM). Each concentration-response curve was normalized to maximal ACh-induced current for each oocyte tested in the absence of the competitive antagonist. X represents substitution for alanine, serine, phenylalanine, or tyrosine.

the α3β2 V7′S and V7′F mutants, respectively. Although no evident changes in antagonist potency are produced by the V7′A and V7′Y mutants (Fig. 7A, Table II). In the case of the apparent potency of the MLA antagonist at the α3β4 receptor, analysis of the data reveals an increase in the apparent potency for all receptor mutants analyzed, with the least degree of change seen with the V7′Y mutant (∼1.8-fold change). The V7′S and V7′F mutations increase antagonist potency at the α3β4 receptor by ∼6.2- and ∼9.3-fold, respectively. In contrast, the V7′A mutation selectively increases the MLA antagonist potency at the α3β4 receptor by ∼18.7-fold (Fig. 7B, Table II). These results suggest that the V7′Y mutation produces lesser to no changes in antagonist potency at the α3β4 and α3β2 receptors, respectively, whereas the V7′S and V7′F mutations increase antagonist potency at both of these receptors.

DISCUSSION

In this study, we investigated the role of the conserved valine residue in position 7′of the putative TMD2 of the neuronal α3 subunit. We selected this position because of its homology to the muscle-type valine 249 residue in which a naturally occurring mutation (V249F) was found to be responsible for a form of SCCMS. Furthermore, this position is highly conserved among neuronal α and β subunits and in the muscle α, δ, and ε subunits. We hypothesized that this position might be critical for appropriate ion channel function.

We substituted position 7′ by four different amino acids. We chose amino acid residues that would alter the amino acid volume but conserve polarity (V7′A and V7′F), residues that would change amino acid volume and polarity (V7′S), and a residue that, as with phenylalanine, would increase the volume but render the posi-

TABLE II. Effect of Mutations at Position α3(V7′) on Competitive Antagonist Sensitivity*

	DHβE				MLA			
nAChR	IC_{50} (μM)	Delta (x)	Apparent K_B (μM)	Delta (x)	IC_{50} (μM)	Delta (x)	Apparent K_B (μM)	Delta (x)
α3β2	0.21 (0.13–0.35)	—	0.22	—	—	—	—	—
α3(V7′A)β2	0.33 (0.21–0.50)	1.57	0.21	0.95	—	—	—	—
α3(V7′S)β2	0.08 (0.04–0.15)	0.38	0.06	0.27	—	—	—	—
α3(V7′F)β2	0.09 (0.04–0.10)	0.43	0.02	0.09	—	—	—	—
α3(V7′Y)β2	0.24 (0.14–0.40)	1.14	0.28	1.27	—	—	—	—
α3β4	—	—	—	—	0.60 (0.42–0.85)	—	0.56	—
α3(V7′A)β4	—	—	—	—	0.05 (0.033–0.08)	0.08	0.03	0.05
α3(V7′S)β4	—	—	—	—	0.17 (0.07–0.30)	0.28	0.09	0.16
α3(V7′F)β4	—	—	—	—	0.13 ± 0.10 (0.08–0.20)	0.22	0.06	0.11
α3(V7′Y)β4	—	—	—	—	0.22 (0.12–0.30)	0.37	0.31	0.55

*Concentration-response curves were obtained after coapplication of 10 μM ACh and increasing concentrations of the appropriate competitive antagonist. IC_{50} values were determined by using Eq. 4. Errors for IC_{50} values are given as the 95% confidence interval of six to 12 individually tested oocytes. Apparent K_B values were calculated by using a modified Cheng-Prusoff equation (Leff and Dougall, 1993).

tion to be less hydrophobic than phenylalanine (V7′Y). There was not a clear, direct relationship between amino acid volume and/or polarity and receptor function. The overall effect of the α3V7′A, α3V7′S, and α3V7′F mutations was to reduce the EC_{50} for ACh and nicotine whether coexpressed with β2 or β4 WT subunits. In contrast, the V7′Y mutation did not cause changes in ACh and nicotine EC_{50} when coexpressed with β2. Coexpression of V7′Y with β4 showed a significant ~1.8-fold increase for ACh and nicotine EC_{50}. In addition to the potentiation of the agonist-induced responses some of the mutant constructs seem to affect channel desensitization, particularly the recovery rate. For example, currents evoked upon successive stimulation displayed a faster peak current rundown in the α3(V7′S)β2 mutant receptor than in the WT. For both receptor subtypes (α3β2 and α3β4), there was an effect of the mutations on the peak current rundown; nonetheless, it is more evident for the mutants coexpressed with the β4 subunit, because the WT α3β4 receptor subtype has no peak current rundown. The α3V7′A, α3V7′S, α3V7′Y, and α3V7′F mutant subunits expressed with the β4 WT subunit showed a significant increase in peak current rundown in comparison with the WT α3β4 receptor subtype. Indeed, the most dramatic effect on peak current rundown was observed for the α3(V7′F)β4 mutant receptor, whereas, for the α3(V7′F)β2 receptor, no statistically significant effect was observed. These results highlight the differential contribution of the β subunit to the mechanism of desensitization (Bohler et al., 2001).

A study by Milone et al. (1997) shows the enhanced desensitization produced by the SCCMS mutation (V249F) in the muscle-type nAChR, and this is consistent with our peak current rundown data. It is important to mention that biochemical studies in the muscle-type nAChR have identified a desensitization "gate" located between residues G240 and L251 (Wilson and Karlin, 2001). Based on the homology between the putative TMDs of muscle and neuronal nAChRs (Sargent, 1993), it is likely that position V7′ of the α3 subunit also contributes to the desensitization of nAChRs.

We also found that position V7′ influences the profile for nicotine pharmacology of the α3 receptor subtypes studied. Previous workers reported that nicotine is a partial agonist of α3β2 but had a better efficacy at α3β4 nAChRs (Wang et al., 1996; Gerzanich et al., 1998; Rush et al., 2002). The partial efficacy of nicotine has been attributed to channel blockade by the agonist and has been shown to be influenced by amino acids at TMD2 and to be voltage dependent (Rush et al., 2002). This voltage dependence of nicotine efficacy for α3β2 has been proposed to arise from the binding of nicotine to a site inside the ion channel that is sensitive to membrane potential. Nicotine has also been reported to induce a voltage-independent blockade of the α3β4 nAChR (Webster et al., 1999). Thus, it was proposed that nicotine blocks the α3β4 nAChR by binding to a site outside the membrane electric field. Consistently with the aforementioned study, we also observed rebound currents at high nicotine concentrations (300 μM) for α3(V7′A)β2, α3(V7′S)β2, α3(V7′A)β4, and α3(V7′S)β4 mutant receptors.

The α3(V7′Y) mutant displayed a remarkably reduced activation for nicotine when coexpressed with both β2 and β4 subunits. Although the ACh activation for this mutant was also reduced, the magnitude for the reduced response for nicotine was ~3-fold larger than for ACh when coexpressed with both β subunits. The dramatic decline in peak current response to nicotine with the tyrosine substitution could have contributions from different effects: reduced nicotine activation (reduced agonist binding), open channel blockade, and desensitization. All of the concentration-dependent curves are normalized to maximal response, so the contribution of block (and desensitization) is not completely evident from the concentration-response relationships. Furthermore, the family of nicotine-induced currents for the V7′Y mutant is dramatically reduced (<500 nA at 300 μM), so the effect of nicotine as a blocker is probably underestimated as a result of the size of the currents. Along the same lines, the notion of nicotine-induced block suggests a second site for the blocker; thus, the interpretation for the contribution of block observed for the V7′Y mutant will depart from the classical notion that ACh and nicotine act at the same site on the receptor. A previous study from our laboratory demonstrated that the properties of agonist binding for channel activation might have distinct dynamics or perhaps structural requirements for ACh and nicotine in the α4β2 neuronal ACh receptor (López-Hernández et al., 2004). This could also be the case for the α3β2 and α3β4 receptors.

A remarkable study by the group of Henry Lester engineered mice hypersensitive to nicotine by the introduction of the M2 α4L9′A mutation (Tapper et al., 2004). This elegant study demonstrated that nicotine activation of the α4 subunit nAChRs was sufficient for reward, tolerance, and sensitization. Along these lines, the pronounced partial agonism for nicotine shown for the α3(V7′Y) mutant in the present study could be used to develop a mutant mouse line with reduced sensitivity to nicotine.

Previous studies had revealed changes in ligand specificity resulting from mutations in TMD2 (Placzek et al., 2004). To test whether mutations at position V7′ affect the sensitivity of the channel to competitive antagonist inhibition, we generated inhibition curves of ACh-elicited current in the presence of different concentrations of two competitive antagonists. We found that most of the mutations studied in this work produced a significant change in the sensitivity to competitive inhibition for most of the α3 receptor subtypes studied. A change in competitive antagonist inhibition would be expected if the mutations were affecting the binding site; our results suggest that this is the case. The concentration-response relationship for a particular agonist is influenced by two independent events, agonist binding and channel gating. Therefore, it is difficult to determine whether changes in EC_{50} are due to an effect of the mutation on binding or perhaps on ion-channel gating (Colquhoun, 1998). A competitive antagonist, however, binds to the receptor binding site but does not trigger receptor activation. Con-

sequently, a mutation that affects channel gating alone should not produce any changes in antagonist IC_{50}. Most of the mutations studied in this work caused a significant change in the sensitivity to competitive inhibition, suggesting that both channel gating and agonist binding are being altered by these mutations.

The current structural model of the receptor locates the TMD2s of the five subunits closely together, forming the inner pore helices and tilting inward toward the central axis (Unwin, 2005). According to this model of the closed state of the *Torpedo* nAChR, position V7′ in the neuronal α3 subunit is oriented toward a water-filled crevice separated from other TMDs. It has been speculated that these crevices between the TMD2s are important in the gating machinery because they provide the necessary space for the TMD2 to move and open the channel pore. Although position V7′ is not predicted to lay in the ion channel pathway, it is very likely that increases in volume or polarity at this position might disturb the rotation of the TMD2 evoked by agonist binding. The largest inhibition of channel gating was observed for the tyrosine replacement. The present data suggest that the hydroxyl group of the tyrosine side chain at position V7′ is decreasing channel function. This inhibition could be due to the formation of a hydrogen bond inside the water crevice between TMD2s. We hypothesize that hydrogen bond formation at this position could increase the energy barrier necessary for the propagation of the conformational wave evoked by agonist binding. In summary, the present study suggests that position V7′ of the neuronal α3 subunit contributes to channel desensitization, pharmacology, and gating.

ACKNOWLEDGMENTS

The authors thank Dr. Walter I. Silva for his valuable input on the pharmacological data. M.N.-C. and M.F.N. were sponsored by the Research Initiative for Scientific Enhancement Program (NIH grant R25GM61151-01A1). D.C.-R. was sponsored by the Louis Stokes Alliance for Minority Participation (LSAMP) Program (NSF grant HRD-0114586) and by the Graduate Assistance in Areas of National Need (GAANN) Program (U.S. Department of Education grant P200A030197-04).

REFERENCES

Bohler S, Gay S, Bertrand S, Corringer PJ, Edelstein SJ, Changeux JP, Bertrand D. 2001. Desensitization of neuronal nicotinic acetylcholine receptors conferred by N-terminal segments of the beta 2 subunit. Biochemistry 40:2066–2074.

Christopoulos A, Grant MKO, Ayoubzadeh N, Kim ON, Sauerberg P, Jeppesen L, El-Fakahany EE. 2001. Synthesis and pharmacological evaluation of dimeric muscarinic acetylcholine receptor agonists. J PET 298: 1260–1268.

Cohen BN, Figl A, Quick MW, Labarca C, Davidson N, Lester HA. 1995. Regions of β2 and β4 responsible for differences between the steady state dose-response relationships of the α3β2 and α3β4 neuronal nicotinic receptors. J Gen Physiol 105:745–764.

Colquhoun D. 1998. Binding, gating, affinity and efficacy: the interpretation of structure-activity relationships for agonists and of the effects of mutating receptors. Br J Pharmacol 125:924–947.

Connolly J, Boulter J, Heinemann SF. 1992. Alpha4-2 beta2 and other nicotinic acetylcholine receptor subtypes as targets of psychoactive and adictive drugs. Br J Pharmacol 105:657–666.

Corringer PJ, Bertrand S, Galzi JL, Devillers-Thiery A, Changeux JP, Bertrand D. 1999. Molecular basis of the charge selectivity of nicotinic acetylcholine receptor and related ligand-gated ion channels. Novartis Found Symp 225:215–230.

Gerzanich V, Wang F, Kuryatov A, Lindstrom J. 1998. Alpha 5 subunit alters desensitization, pharmacology, Ca^{2+} permeability and Ca^{2+} modulation of human neuronal alpha 3 nicotinic receptors. J Pharmacol Exp Ther 286:311–320.

Karlin A. 2002. Emerging structure of the nicotinic acetylcholine receptors. Nat Rev Neurosci 3:102–114.

Kuryatov A, Gerzanich V, Nelson M, Olale F, Lindstrom J. 1997. Mutation causing autosomal dominant nocturnal frontal lobe epilepsy alters Ca^{2+} permeability, conductance, and gating of human alpha4beta2 nicotinic acetylcholine receptors. J Neurosci 17:9035–9047.

Leff P, Dougall IG. 1993. Further concerns over Cheng-Prusoff analysis. Trends Pharmacol Sci 14:110–112.

López-Hernández GY, Sánchez-Padilla J, Ortíz-Acevedo A, Lizardi-Ortíz J, Salas-Vincenty J, Rojas LV, Lasalde-Dominicci JA. 2004. Nicotine-induced up-regulation and desensitization of α4β2 neuronal nicotinic receptors depend on subunit ratio. J Biol Chem 279:38007–38015.

Milone M, Wang HL, Ohno K, Fukudome T, Pruitt JN, Bren N, Sine SM, Engel AG. 1997. Slow-channel myasthenic syndrome caused by enhanced activation, desensitization, and agonist binding affinity attributable to mutation in the M2 domain of the acetylcholine receptor alpha subunit. J Neurosci 17:5651–5665.

Nelson ME, Lindstrom J. 1999. Single channel properties of human alpha3 AChRs: impact of beta2, beta4 and alpha5 subunits. J Physiol 516:657–678.

Ohno K, Engel AG. 2002. Congenital myasthenic syndromes: genetic defects of the neuromuscular junction. Curr Neurol Neurosci Rep 2:78–88.

Ortíz-Acevedo A, Meléndez M, Asseo AM, Biaggi N, Rojas LV, Lasalde-Dominicci JA. 2004. Tryptophan scanning mutagenesis of the γM4 transmembrane domain of the acetylcholine receptor from *Torpedo californica*. J Biol Chem 279:42250–42257.

Placzek AN, Grassi F, Papke T, Meyer EM, Papke RL. 2004. A single point mutation confers properties of the muscle-type nicotinic acetylcholine receptor to homomeric alpha7 receptors. Mol Pharmacol 66:169–177.

Rush R, Kuryatov A, Nelson ME, Lindstrom J. 2002. First and second transmembrane segments of alpha3, alpha4, beta2, and beta4 nicotinic acetylcholine receptor subunits influence the efficacy and potency of nicotine. Mol Pharmacol 61:1416–1422.

Sargent PB. 1993. The diversity of neuronal nicotinic acetylcholine receptors. Annu Rev Neurosci 16:403–443.

Tapper AR, McKinney SL, Nashmi R, Schwarz J, Deshpande P, Labarca C, Whiteaker P, Marks MJ, Collins AC, Lester HA. 2004. Nicotine activation of α4* receptors: sufficient for reward, tolerance, and sensitization. Science 306:1029–1032.

Unwin N. 2005. Refined structure of the nicotinic acetylcholine receptor at 4Å resolution. J Mol Biol 346:967–989.

Wang F, Gerzanich V, Wells GB, Anand R, Peng X, Keyser K, Lindstrom J. 1996. Assembly of human neuronal nicotinic receptor alpha5 subunits with alpha3, beta2, and beta4 subunits. J Biol Chem 271:17656–17665.

Webster JC, Francis MM, Porter JK, Robinson G, Stokes C, Horenstein B, Papke RL. 1999. Antagonist activities of mecamylamine and nicotine show reciprocal dependence on beta subunit sequence in the second transmembrane domain. Br J Pharmacol 127:1337–1348.

Wilson G, Karlin A. 2001. Acetylcholine receptor channel structure in the resting, open, and desensitized states probed with the substituted-cysteine-accessibility method. Proc Natl Acad Sci U S A 98:1241–1248.